# End-wall effects in granular tumblers: From quasi-two-dimensional flow to three-dimensional flow

Nicholas A. Pohlman, Julio M. Ottino, and Richard M. Lueptow*
*Northwestern University, Evanston, Illinois 60208, USA*
(Received 2 February 2006; published 19 September 2006)

The flow of granular material in rotating tumblers is confined to a thin flowing layer at the free surface in which the particle velocity is primarily streamwise, perpendicular to the axis of rotation, with minimal axial motion. Particle tracking velocimetry was used to measure the surface velocity for 1 and 2 mm glass particles and sand in cylindrical tumblers of various diameters, lengths, and rotation rates for a flat continuously flowing surface. End-wall friction slows the streamwise surface velocity adjacent to the walls, yet material just inward from the end wall flows faster than the material in the center of a long tumbler. An axial velocity occurs near the end walls both upstream and downstream of the midlength of the flowing layer. Increasing the tumbler diameter and corresponding flowing layer length causes the magnitude of the axial and streamwise velocity components, as well as the axial thickness of the end-wall region, to increase. An increase of end-wall friction slows particles directly adjacent to the end wall, further enhancing the axial flow near the end wall. Increasing the rotation rate, while still maintaining a flat continuously flowing surface, causes a corresponding increase in both the streamwise and axial velocities in the tumbler. The boundary flow effects are localized to end walls when the axial length of the tumbler ($L$) is greater than the diameter ($D$), so that the flow in the center region of the tumbler is independent of the end walls and hence similar to the conditions at the center of an infinitely long tumbler. Decreasing the axial length of the tumbler so that $L/D<1$ causes the axial velocity to decrease as the regions affected by the end walls merge. This also leads to a streamwise velocity in quasi-two-dimensional tumblers that can be more than twice that at the center of three-dimensional tumblers.

DOI: 10.1103/PhysRevE.74.031305 PACS number(s): 45.70.−n, 47.57.Gc

## I. INTRODUCTION

Granular flow in a rotating tumbler is a canonical system for the study of segregation and mixing as well as the general flow properties of granular materials. Most studies of granular tumbler flow have neglected the effects of the end-wall boundaries on the flow. Recent studies indicate that granular flow near end-wall boundaries is different from the flow observed far from end walls for both chute flow and rotating tumbler flow [1–4]. In particular, regions of higher streamwise velocity have been observed near the end walls that appear to be a result of the frictional influence of the end walls [2,4]. Furthermore, experiments using bidisperse particles in long tumblers indicate that end-wall effects can initiate axial band formation or result in curved interfaces between bands of segregated particles near the end walls [5–11]. Conversely, mixing experiments of monodisperse particles indicate that mixing is faster close to the end walls than at the center of the tumbler [12].

Santomaso *et al.* [12] suggested that particles follow streamlines near the end walls of rotating tumblers that curve away from the end wall in the upstream portion of the flowing layer and back toward the end wall in the downstream portion. Recent preliminary experiments indicate that the axial velocity near the end walls can be significant upstream and downstream of the midlength of the flowing layer even though the axial flow is negligible at the midlength [4]. In addition, higher streamwise velocities occur near the end walls than at the center of rotating tumblers [2,4]. The explanation for this is based on the conservation of mass [3,4]. All of the particles in the fixed bed must pass through the flowing layer every half-revolution for a half-full tumbler. Frictional interaction with the end wall results in slower streamwise velocity immediately adjacent to the end wall. Since the flux of particles entering the flowing layer is the same adjacent to the end walls as it is elsewhere in the tumbler, the particles in the flowing layer near the end wall must compensate for the lower mass flux due to wall friction. To do so, they flow away from the end wall in the upstream portion of the flowing layer, and then flow down the slope faster than particles at the end wall. In the downstream portion of the flowing layer, the particles flow back toward the end wall to conserve mass, since the flux of slower particles next to the end wall is inadequate to fill the fixed bed.

In this paper, we consider the flow of particles of diameter $d$ in half-full circular tumblers of diameter $D=2R$ and length $L=2H$ rotating at $\omega$, as shown schematically in Fig. 1, so that there is a continuously flowing layer with a flat free surface. The coordinate system is positioned at the center of the length of the tumbler on the axis of rotation with the $x$-$z$ plane at the free surface of the flow and the $y$ axis normal to it. The velocities are $u$ (streamwise), $v$ (normal), and $w$ (spanwise or axial), with the predominant flow in the streamwise direction.

An unavoidable difficulty in the measurement of granular flow is the opacity of the particles that limits observation to the free surface or end walls of the container. As a result, many experiments have been conducted under quasi-two-dimensional conditions to measure the streamwise particle velocity profiles, $u(y)$, through the depth of the flowing layer [13–20]. The highest streamwise velocity occurs at the free

*Electronic address: r-lueptow@northwestern.edu

 

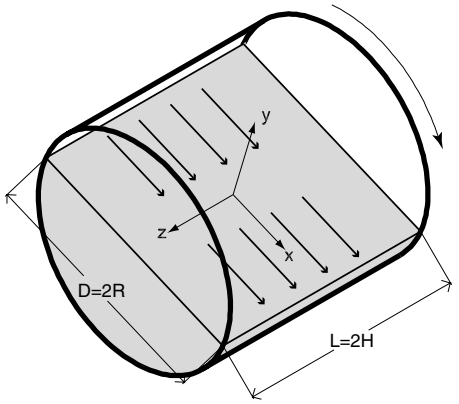


FIG. 1. Three-dimensional rotating tumbler with 50% fill of granular material (shaded region).

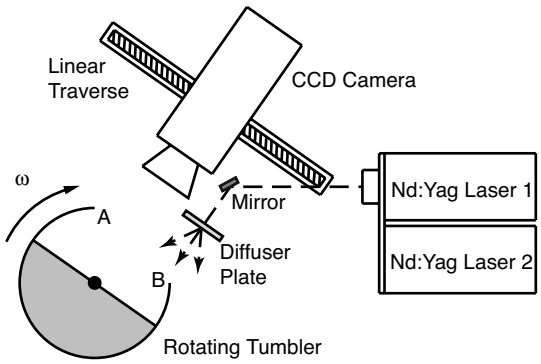


FIG. 2. Schematic of the half-full rotating tumbler showing the CCD camera, linear traverse, and Nd:YAG laser light source with redirecting mirror and diffuser plate (not to scale).

surface of the flow with the velocity decreasing to near zero at a depth of $5d$ to $10d$ for millimeter-sized spherical beads [3,21]. Other methods have been developed to measure the flow beneath the visible surface and far from end walls in three-dimensional rotating tumblers (magnetic resonance imaging [3,22], fiber optic probes [2], and positron emission particle tracking [23]). Although these techniques permit measurement of the velocity below the surface of a granular flow, the methods often lack spatial and/or temporal resolution. Nevertheless, similar conclusions have been drawn from these measurements as were obtained from quasi-2D measurements regarding the streamwise velocity profile through the depth of the flowing layer. Optical methods have been used in 3D tumblers to measure the particle velocity at the free surface of the flowing layer. This previous work was focused on the streamwise velocity as a function of a single coordinate, either the position along the flowing layer, $u(x)$ [24], or the axial position at the midlength of the flowing layer, $u(x=0,z)$ [4].

Although curved particle trajectories have been hypothesized near the end walls [12], experiments have not been performed to quantify this flow. Only by measuring both components of the surface velocity (streamwise and spanwise) can the effects of the end-wall boundaries of the tumbler be investigated. Perhaps more important is the question of the relation between the flow in quasi-two-dimensional tumblers with an axial length of a few particle diameters and the flow in long tumblers. In the first case, the end walls play a major role in constraining the flow, whereas for long tumblers, the impact of the boundary flow is likely to be localized to regions near the end walls. However, it is unclear how far away from the end walls their impact extends. In addition, it is unclear how narrow the tumbler must be before the flow becomes quasi-two-dimensional. For that matter, to what extent does flow in a quasi-2D tumbler capture the flow in a cross section of a 3D tumbler? In this work, we measure the streamwise and axial velocity components over the entire free surface of the flowing layer in tumblers of varying axial length ($L$), diameter ($D$), and rotation rate ($\omega$), as well as for different particle sizes ($d$). The objective is to understand better the impact of end-wall boundaries on granular flow in quasi-two-dimensional and three-dimensional circular tumblers.

## II. EXPERIMENTAL METHODS

The velocities of particles at the free surface of the rotating tumbler were measured using particle tracking velocimetry (PTV). Due to the curvature of the cylindrical container, distortion of particle locations would be induced if images were taken through a transparent cylinder. To eliminate this error source, a quarter sector of a cylinder was removed to provide undistorted visibility of the free surface, as shown in Fig. 2. To begin an experiment, the tumbler was rotated counterclockwise until particles reached edge **A**. Data were obtained as the tumbler rotated clockwise and the field of view of the camera was between edges **A** and **B**. Rotation and image acquisition were stopped just prior to the particles reaching edge **B**. The transient dynamics of starting the system from rest were verified to decay in less than 2 s after the initial onset of flow [4]. Image acquisition was started only after the flow reached a steady state.

Cylindrical tumblers were constructed from acrylic tubes of various diameters and axial lengths with acrylic end walls. Tumblers with a $D=17.0$ cm diameter had axial lengths of $L=1.0$, 2.3, 4.4, 8.8, and 17.5 cm providing $L/D$ ratios of 0.06, 0.14, 0.26, 0.52, and 1.03, respectively. The maximum axial length of $L=17.5$ cm was also tested for cylinder diameters of $D=7.0$, 10.0, and 14.0 cm. A long cylinder with $L=70.0$ cm and $D=14.0$ cm was used to verify that $L=17.5$ cm was a sufficient length to avoid end-wall effects in the center of the tumbler. Some tests were performed with 100-grit sandpaper attached to the end walls of the $L/D=1.03$ tumbler to determine the influence of increased end-wall friction on the free surface flow. All interior acrylic surfaces of the tumblers were cleaned with an antistatic wipe prior to filling with granular material. Rotation rates of 1.0, 2.0, and 3.5 rpm were controlled with a dc stepper motor. The operating conditions provided an order of magnitude change of the Froude number ($\mathrm{Fr}=R\omega^2 g^{-1}$), which represents the ratio of the centrifugal force to the gravitational force. The range of Froude numbers ($9.5\times10^{-5}<\mathrm{Fr}<1.2$

$\times 10^{-3}$) was such that the continuously flowing free surface remained flat.

Experiments were conducted with a fill level of 50% for one of two particle types: black basalt spherical glass beads ($\rho=2.6$ g cm$^{-3}$) of two sizes, $d=1.07\pm0.04$ mm or $d=2.03\pm0.03$ mm, or black art sand that passed through a 0.5 mm screen. Thus, for the sizes of beads that were used, the axial length of the tumbler ranged from $L=5d$ (quasi-two-dimensional) to $L=654d$. The particles at the free surface were made visible with a flash from a 25 mJ Nd:YAG laser (New Wave Research). A mirror redirected the laser beam normal to the face of a diffuser plate held stationary and parallel to the dynamic angle of repose. The laser flash was synchronized with a 1 megapixel charged coupled device (CCD) camera (TSI, Inc.) to illuminate particle locations. The field of view for an individual image was approximately 3.5 cm. The camera was mounted on a linear traverse that was parallel to the free surface. The traverse was used to translate the camera in the flow direction ($x$ axis) in order to obtain images for most of the length of the flowing layer without having to adjust the focal plane of the camera. It was not possible to make measurements near the extrema of the length of the flowing layer due to the occlusion of edges **A** and **B** of the tumbler. The tumbler assembly was moved axially to position different sections of the tumbler below the camera. In this way, a mosaic of images of the particle motion across the entire surface of the flowing layer was obtained.

Image pairs separated by 2.5–10 ms were obtained at 15 Hz. Velocity estimates of the free surface were computed using particle image velocimetry (PIV) software (*Insight*, TSI, Inc.). The estimates were then used in conjunction with PTV software to measure the velocities of individual particles based on a single bright spot on each particle [18,25]. Due to the reflective nature of the acrylic tumbler, some particles near the end walls had multiple bright spots of reflected light. The double reflection actually aided the PTV algorithm by providing a better cross correlation than the single spot per particle available in the center of the tumblers. Errors due to the translation of the spectral reflection of the bright spot on an individual particle between image pairs produced a potential velocity bias of less than 0.5%. The subpixel resolution of reflected points between image pairs resulted in an error of less than 1% in the velocity for individual particles.

Images could only be obtained within the cutout of the tumbler for a limited time between the start of a steady flow condition and the free surface being occluded by the cylinder walls. Multiple runs were conducted in order to obtain at least 100 image pairs for each measurement position. No differences in the flow dynamics occurred from the first images to the last images, indicating that the initial conditions were nearly identical for all the runs. Individual vectors from all of the image pairs were binned into square regions that were three particle diameters long and wide. Typically, each bin contained more than 200 vectors. Vectors more than five standard deviations from the mean were recursively removed, eliminating less than 0.2% of all available vectors.

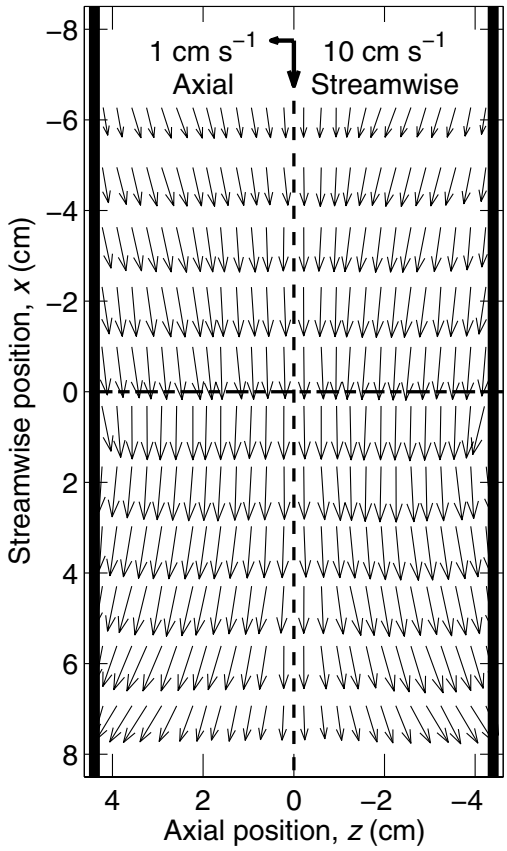


FIG. 3. Velocity field at the surface (to scale) of the $L/D=0.52$ tumbler rotated at 2.0 rpm (Fr$=3.8\times10^{-4}$) for 1 mm particles. The bold vertical lines indicate the end walls of the cylindrical tumbler; the vertical dashed line is the axial center of the tumbler at $z=0$; the horizontal dashed line is the axis of rotation at $x=0$. The axial components of the vectors are scaled by a factor of 5 relative to the streamwise components (see bold vectors at the top). The axial position extends from positive values on the left to negative values on the right to be consistent with looking down onto the free surface as indicated in Fig. 1.

## III. RESULTS

### A. Free surface velocity field

The average velocity field of the free surface is shown in Fig. 3 for the $L/D=0.52$ tumbler with 1 mm particles rotated at 2.0 rpm (Fr$=3.8\times10^{-4}$). Only 25% of the measured vectors in the streamwise direction are shown in order to avoid overlapping vectors. The curved particle velocity field is immediately evident, although the axial velocity component is exaggerated so it is not dwarfed by the large streamwise velocity component. In the upstream portion of the flowing layer, the particles tend to move toward the center of the tumbler, away from the end wall. At the midlength of the flowing layer ($x=0$), the axial velocity component becomes negligible, as has been previously reported [4]. In the downstream region, particles move back toward the end wall to satisfy conservation of mass. These results confirm that the curved particle trajectories that have been hypothesized [3,4,12] do indeed occur. The flow field is symmetric about the $z$ axis (the axial center of the tumbler), and the axial

velocity component is zero at this axial position. From this initial experiment, it is unclear if this is a result of the symmetry of the end-wall conditions or a result of the end-wall effects extending only a few centimeters from the end walls.

Of course, the velocity field in Fig. 3 shows the general flow of the particles down the slope of the free surface. The streamwise velocity is slow in the upstream portion of the flowing layer, increases to a higher velocity through the midlength of the flowing layer, and then decreases in the downstream portion. This is consistent with previous results for a continuously flowing layer with a flat surface in tumblers at similar Froude numbers [2,22,24]. Additionally, the streamwise velocity adjacent to the end wall is slower than the velocity closer to the center of the tumbler similar to previous experiments conducted in much narrower rotating tumblers [3]. The average standard deviation of the velocity, which is indicative of diffusive velocity fluctuations, is $1.5 \pm 0.2$ cm s$^{-1}$ for the streamwise velocity and $1.1 \pm 0.2$ cm s$^{-1}$ for the spanwise (axial) velocity. Similar results occur for 2 mm particles at the same operating conditions, albeit with larger velocity fluctuations of $2.1 \pm 0.2$ cm s$^{-1}$ for the streamwise component and $1.5 \pm 0.1$ cm s$^{-1}$ for the axial component. The values for the standard deviation reflect that the diffusion scales approximately with $d^{1/2}$, consistent with theory and previous results [4].

### B. Flow variation due to tumbler parameters

The influence of the rotating tumbler's operating conditions on the axial velocities is shown more clearly in Fig. 4, where the axial velocity contours are shown for a wide range of tumbler lengths, diameters, and rotation rates. The intensity corresponds to the magnitude of the axial velocity. The orientation of the tumblers is the same as that shown in Fig. 3, so that the direction of flow is from top to bottom. The axial velocity is away from the end wall in the upper left and right quadrants, while it is toward the end wall in the lower left and right quadrants. The contours are shown for a rotation rate of 2 rpm, except for the $L/D=0.26$ tumbler (c), for which contours for rotation rates of 1.0, 2.0, and 3.5 rpm are shown.

From Fig. 4 it is evident that the axial velocity magnitude depends on the tumbler size and operating conditions. Similar results occur for 2 mm particles, as shown in Fig. 5. The influence of each operating parameter on the free surface flow is discussed individually in the following sections.

#### 1. Variation of tumbler length

A key question is how long does the tumbler need to be before there is a region at the center of the tumbler where end walls do not affect the flow? The top row of contour plots in Figs. [(a)–(e)] for tumblers of diameter $D=17.0$ cm shows the regions in which there is an axial flow due to the proximity of the end walls. These regions extend to the center of the tumbler for $L/D \leqslant 0.52$ [(a)–(d)]. Only when $L/D=1.03$ (e) is there a region where zero axial flow extends away from the center of the tumbler. The similarity of the axial extent of the shaded regions in the top row of Figs. 4

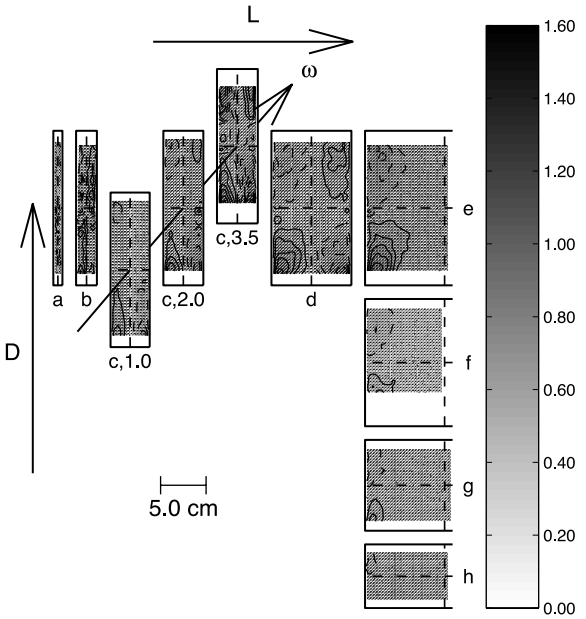


FIG. 4. Intensity of the axial velocity component in cm s$^{-1}$ for 1 mm particles in the following rotating tumblers that are drawn to scale: (a) $L/D=0.06$, (b) $L/D=0.14$, (c) $L/D=0.26$ at the rotation rate specified, (d) $L/D=0.52$, (e) $L/D=1.03$, (f) $L/D=1.25$, (g) $L/D=1.75$, and (h) $L/D=2.5$. Contours represent steps of 0.2 cm s$^{-1}$; dashed contours are negative; solid contours are positive. The solid lines outline the area of the free surface as limited by the end walls and the radial extent of the cylindrical tumblers; the vertical dashed lines are the axial centers of the tumbler at $z=0$; the horizontal dashed lines are the axes of rotation at $x=0$. For longer tumblers, only flow in the positive $z$ half of the tumbler was measured. The relative sizes of the tumblers are to scale. Images are unavailable at the downstream edge of the 14.0 cm-diam cylinder ($f$) due to the angle of the cut on edge **B** in Fig. 2 occluding the camera's view. Intensity scaling is identical to that shown in Fig. 5.

and 5 indicates that the distance that the boundary flow extends from the end walls is related to the geometry of the tumbler and only depends on the particle size for the narrowest axial lengths. Differences occur in the narrow tumblers [(a) and (b)] when the granular material changes from 1 and 2 mm particles. This is likely due to the number of particles that span the fixed axial length for the two different particle sizes. For example, in the $L/D=0.06$ tumbler (a), the axial length is 10 particle diameters for 1 mm beads and 5 particle diameters for the 2 mm beads. At longer axial lengths, the overall axial dimension is dominant.

From these figures it also appears that the axial velocity increases (darker shading and more contours) as the length of the tumbler increases. This is shown more clearly in Figs. 6(a) and 6(b), in which the axial velocity is plotted as a function of the nondimensional axial position for 1 mm particles rotated at 2 rpm in tumblers of different axial lengths. The characteristic velocity used for scaling is assumed to be of the form $R/\tau$, where $\tau$ is a characteristic time scale. Several time scales are available: (i) $1/\omega$, which is at the level of the tumbler system; (ii) $1/\dot{\gamma}$, where $\dot{\gamma}$ is the shear rate through the depth, which is at the level of the flowing layer (this is unavailable since measurements are only at the sur-

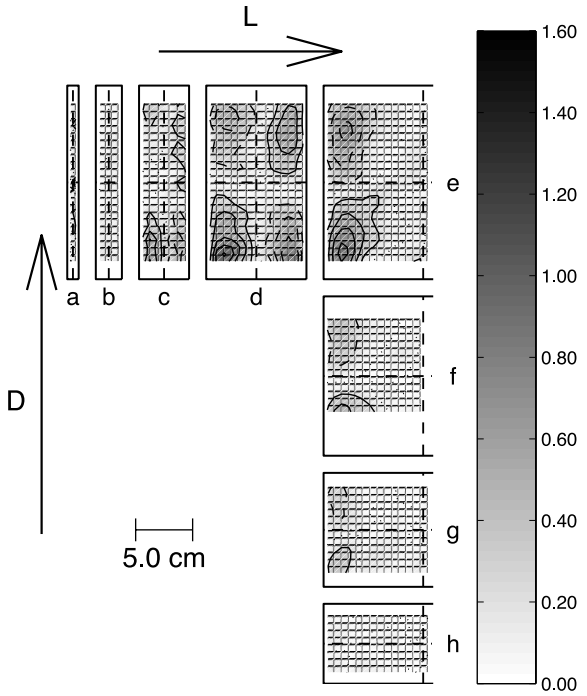


FIG. 5. Intensity of axial velocity component in cm $s^{-1}$ of 2 mm particles for the following sizes: (a) $L/D=0.06$, (b) $L/D=0.14$, (c) $L/D=0.26$, (d) $L/D=0.52$, (e) $L/D=1.03$, (f) $L/D=1.25$, (g) $L/D=1.75$, and (h) $L/D=2.5$. Variation in the rotation rate was not tested for this particle size. Line conventions and intensity scaling are the same as Fig. 4.

face); and (iii) $\sqrt{d/g}$, which is at the particle level. The velocity is nondimensionalized here using the linear speed of the edge of the rotating tumbler ($\omega R$), but an alternative is explored later in this paper. The streamwise locations for the velocity profiles are $x/R=\pm 0.75$, to correspond to the positions near which the maximum axial velocity occurs. Particles in the upstream region of the flowing layer at $x/R=-0.75$ [Fig. 6(a)] are moving toward the center of the tumbler ($w>0$ for $z/H<0$ and $w<0$ for $z/H>0$) with a negligible spanwise velocity at the center of the tumbler ($z/H=0$). The overall form is symmetric, although there are inherent fluctuations in axial velocity measurements. The two longest tumbler lengths have different profiles than the shorter tumblers, because the boundary flow is localized near the end wall and does not influence the surface velocity at the center of the tumbler. Figure 6(b) shows data at the symmetrically opposite downstream region of the flowing layer at $x/R=0.75$. The profiles exhibit an approximate antisymmetry with those of Fig. 6(a), since the particles are moving back toward the end walls. The axial flow back toward the end wall is stronger than the flow away from the end wall, most likely due to the asymmetry of the streamwise velocity profile discussed shortly.

Figures 7(a) and 7(b) show the streamwise velocity profiles as a function of the axial position for tumblers of different lengths rotated at 2.0 rpm with 1 mm particles. The streamwise velocities are an order of magnitude or more greater than the axial velocities, shown in Fig. 6. The dependence of the streamwise velocity profile, $u(x/R=0,z/H)/(\omega R)$, on the tumbler length shown in Fig. 7(a) appears similar to that observed for surface flow in chutes of varying width in that the streamwise velocity increases as the width between the walls decreases [1]. Figure 7(b) replots the streamwise velocity profile normalized by the "free stream" surface velocity at the axial center ($x/R=0$, $z/H=0$) in order to allow comparison of the shape of the velocity profiles. In the long tumblers, there is a sharp increase in streamwise velocity near the end walls that is most prominent for the longest tumbler ($L/D=1.03$) and less evident for the next longest tumbler ($L/D=0.52$). Conversely, in the shorter tumblers ($L/D<0.52$), the maximum velocity is at the axial center of the tumbler. This is different from the fully developed flow observed in chutes where, regardless of the chute width, the maximum velocity is always in the center, and particles adjacent to the side wall move slower [1]. For the flow in a chute, the thickness of the side wall boundary flow can grow along the length of the chute until the two boundary flows merge resulting in the maximum streamwise velocity at the center of the chute. In a rotating tumbler, the length of the flowing layer is limited to the diameter of the tumbler. As a result, rotating tumblers continuously reset the

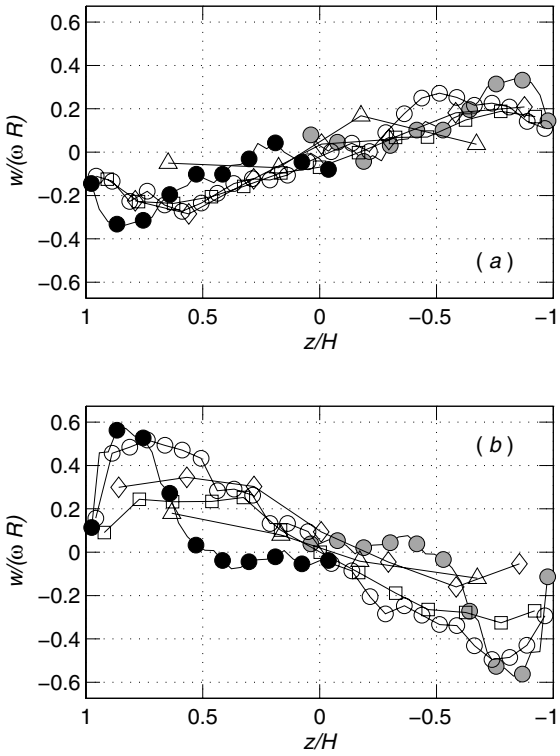


FIG. 6. The axial velocity profile along the axial position in the upstream and downstream regions of the flow for 1 mm particles in tumblers rotated at 2.0 rpm: (a) upstream at $x/R=-0.75$; (b) downstream at $x/R=0.75$. All cylinders have a diameter of $D=17.0$ cm. Symbols represent the following axial length to diameter ratios: △, $L/D=0.06$; ◇, $L/D=0.14$; □, $L/D=0.26$; ○, $L/D=0.52$; and ●, $L/D=1.03$. (Only every third data point for $L/D=1.03$ is indicated with a marker to aid in the clarity of the figure; these data are also reflected across the axial line of symmetry and shown in gray fill.) The horizontal axis extends from 1 to −1 from left to right to be consistent with the $z$ axis in Fig. 3.

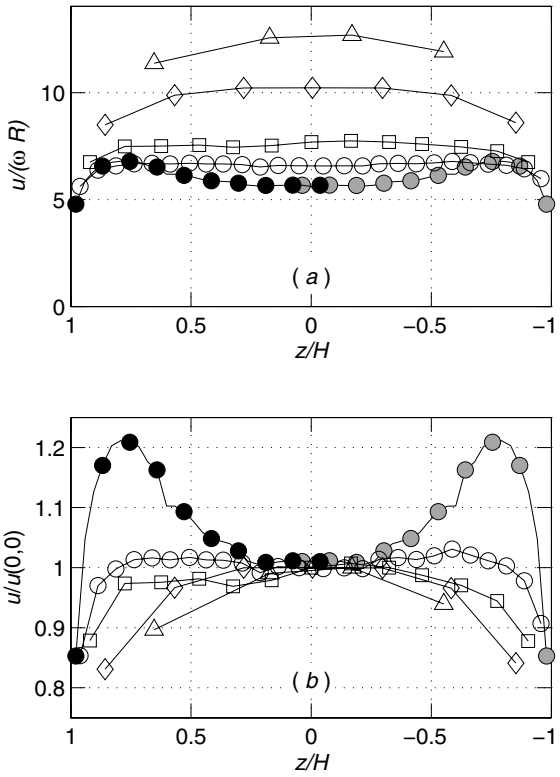


FIG. 7. The streamwise surface velocity as a function of the axial position in the $D=17.0$ cm cylindrical tumblers at the midlength of the flowing layer ($x/R=0$) for 1 mm particles in tumblers rotated at 2.0 rpm. (a) Streamwise velocity; (b) streamwise velocity normalized by $u(x/R=0,z/H=0)$. Symbols represent the following axial length to diameter ratios: △, $L/D=0.06$; ◇, $L/D=0.14$; □, $L/D=0.26$; ○, $L/D=0.52$; and ●, $L/D=1.03$.

boundary flow condition at the beginning and end of the flowing layer as particles exit and enter the fixed bed of material. Since the boundary flow cannot continuously grow in width, a higher streamwise velocity occurs near the end wall to accommodate the flux of particles entering the flowing layer.

The dependence of the streamwise surface velocity profile on the position along the flowing layer at the axial center of the tumbler, $u(x/R,z/H=0)$, is approximately parabolic for all of the cylinder lengths, similar to previous results [2,23,24], as shown in Fig. 8 for both glass particle sizes. Here, the velocity is nondimensionalized in two ways: the top row shows velocity of (a) 1 mm particles and (b) 2 mm particles nondimensionalized using the system level time scale $1/\omega$; the scaling for the bottom row incorporates the particle level time scale $\sqrt{d/g}$ for (c) 1 mm particles and (d) 2 mm particles. With either scaling, the highest velocities occur in the narrowest tumblers. When the velocity is scaled by $\omega R$, the 1 mm particles reach a higher streamwise surface velocity in the narrower tumblers than the 2 mm particles [upper profiles in (a) and (b)]. The velocity profiles for the two particle sizes are very similar when the axial length is large [lower profiles in (a) and (b)]. The difference in the velocity profiles for the narrowest tumblers (upper profiles) suggests that system level time scales do not characterize the velocity when the axial length is small. However, the particle level scaling using $\sqrt{g/dR}$ results in similar magnitudes for the narrowest tumblers [upper profiles in (c) and (d)], though the magnitudes for longer tumblers differ substantially (lower profiles). This result is not surprising given that the axial dimension is approaching the length of a few particle diameters for narrow tumblers.

The streamwise velocity profiles are asymmetric with respect to the midlength of the flowing layer as particles continue to accelerate past this point. This acceleration beyond the midlength of the flowing layer likely contributes to the higher axial velocity in the downstream region of flow in Fig. 6(b) than in the upstream region in Fig. 6(a). Since particles accelerate beyond the midlength of the flowing layer, there is a shorter downstream distance available for the particles to move back toward the end walls, thus increasing the downstream axial flow. The maximum streamwise ve-

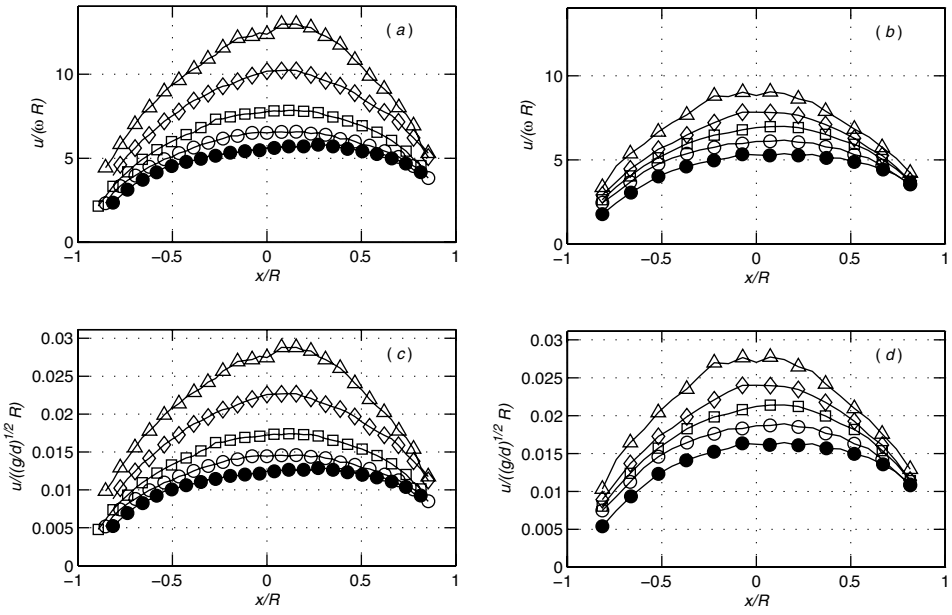


FIG. 8. The streamwise surface velocity along the flowing layer at the axial center ($z/H=0$) for $D=17.0$ cm cylindrical tumblers rotated at 2.0 rpm with 1 mm (left column) and 2 mm (right column) particles. The top row scales the streamwise velocity by $\omega R$ while the bottom row is nondimensionalized by $\sqrt{g/dR}$. (Only every other data point is indicated with a marker to aid in the clarity of the figures.) Symbols are the same as in Fig. 6.

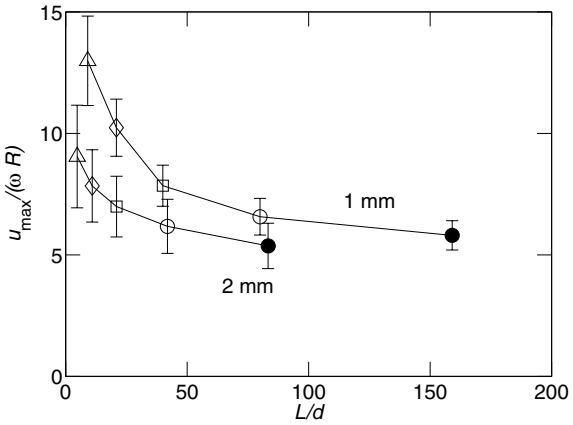


FIG. 9. The relationship between maximum streamwise surface velocity at the center of the tumbler and the length of the rotating tumbler (in terms of the number of particle diameters) for 1 and 2 mm particles with the average standard deviation given by the error bars. Symbols are the same as in Fig. 6.

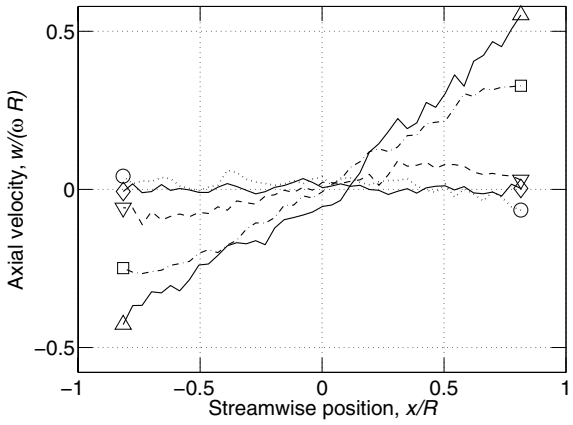


FIG. 10. Axial velocity profiles along the direction of the flowing layer for 1 mm particles rotated at 2.0 rpm in the $L/D=1.03$ tumbler. Symbols at the end points of the individual profiles represent the following axial locations: △ with solid curve, $z/H=0.90$ (near the end wall); □ with dash-dot curve, $z/H=0.67$; ▽ with dashed curve, $z/H=0.46$; ○ with dotted curve, $z/H=0.23$; ◇ and with solid curve, $z/H=0.0$ (center of the tumbler).

locities based on a parabolic curve fit for each profile occur at $x/R=0.04$, 0.07, 0.08, 0.09, and 0.15 for $L/D=0.06$, 0.14, 0.26, 0.52, and 1.03, respectively, for 1 mm particles and $x/R=0.02$, 0.05, 0.07, 0.07, and 0.13 for the same axial lengths with 2 mm particles. The increase in skewness as a function of the axial length of the container indicates that particles accelerate further beyond the midlength in longer tumblers much like what occurs as the flowing layer length increases with increasing radius of the tumbler [24]. This can be explained in terms of the reduced impact of the friction of distant end walls allowing the distance that a particle accelerates through the flowing layer to increase.

Regardless of the acceleration distance, narrower tumblers have higher streamwise velocities. In fact, the maximum streamwise velocity at the axial center of the tumbler decays approximately exponentially with the axial length of a tumbler asymptoting to a value of about $5\omega R$, as shown in Fig. 9. The maximum streamwise velocity for the quasi-two-dimensional case ($L/D=0.06$) is 124% greater for 1 mm particles and 70% greater for 2 mm particles than for the fully three-dimensional tumbler ($L/D=1.03$). Of course, the streamwise surface velocity does not continue to increase as $L/d$ gets smaller, because eventually the distance between end walls is small enough that packing influences the flow properties. The higher velocity for short tumblers in Figs. 8 and 9 is likely a result of the lack of available axial space for spanwise flow. In addition, the proximity of the end walls may result in more dilation of the flowing layer than occurs in the center of a longer tumbler, because the wall exclusion effect reduces the packing density. In either case, conservation of mass requires that all of the particles must pass through the flowing layer every one-half revolution for a half-full tumbler. Of course, the particles very near the end walls are slowed by friction. Thus, either the flowing layer depth must increase or the streamwise velocity must be greater, as seems to be the case.

This demonstrates an important difference in the flow conditions between quasi-2D tumblers and fully 3D tumblers. Returning to the top row of Figs. 4 and 5, the contours for $L/D=0.52$ (d) have magnitudes similar to those for $L/D=1.03$ (e). However, the boundary flow effect in the longer tumbler is localized near the end wall with negligible axial flow in the center of the tumbler. To be sure that the end-wall flows were not interacting with each other, experiments were also conducted in a 14.0-cm-diam cylinder that was 70.0 cm long ($L/D=5.0$) and rotated at 2.0 rpm. The results confirmed that the axial flow is indeed localized to the end wall with negligible axial flow only a few centimeters away. This result along with the proximity of the contours in the top rows of Figs. 4 and 5 to the end walls of the tumblers suggests that the axial length of a tumbler must be such that $L>D$ so that the flows near the end walls are localized to an individual end wall and not interacting with each other. The limited axial length in narrow containers forces the boundary flows to merge creating a flowing layer that increases its streamwise velocity rather than generating axial flow to conserve mass.

For the case of a long cylinder where the end-wall flows do not merge, the maximum axial velocity magnitudes occur closest to the end walls. Figure 10 shows the axial velocity profiles with respect to the flowing layer position for different axial locations in the $L/D=1.03$ tumbler. Because of the substantial fluctuations in the axial velocity measurements, the data are smoothed using Fourier methods to provide clearer velocity profiles. Negative and positive velocities indicate flow away from and toward the end wall, respectively. Again, it is evident that the axial velocity is larger in the downstream portion of the flowing layer than in the upstream portion. Profiles closer to the axial center of the tumbler exhibit a reduced axial velocity indicating the localized effect of the end-wall boundary. The maximum magnitude of the dimensionless axial velocity near the end wall is 0.62. For comparison, the mean of the dimensionless axial velocity standard deviations along the length of the flowing layer at the center of the tumbler, which provides some indication of the diffusional velocity, is 0.45. The similarity in the magni-

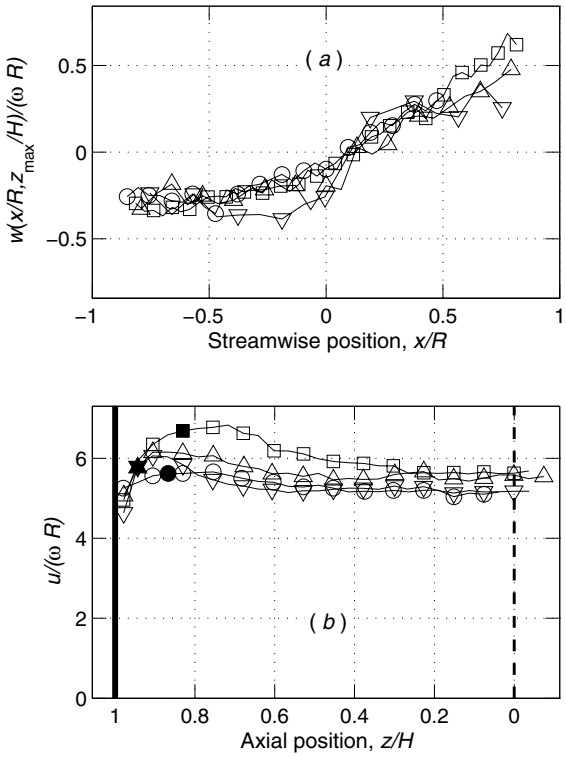


FIG. 11. (a) Axial velocity along the flowing layer at the axial position where the highest axial velocity occurs, $w(x/R, z_{\max}/H)$, and (b) streamwise velocity profile at the midlength of the flowing layer, $u(x/R=0, z/H)$, for $L=17.5$ cm tumblers rotated at 2.0 rpm for 1 mm particles. Symbols indicate the cylinder diameter: ▽, 7.0 cm ($L/D=2.5$); △, 10.0 cm ($L/D=1.75$); ○, 14.0 cm ($L/D=1.25$); and □, 17.0 cm ($L/D=1.03$). (Only every other data point is indicated with a marker to aid in the clarity of the figure.)

tude of the diffusional velocity and the advective axial velocity near the end walls suggests that the axial flow near end walls is indeed large enough to cause the enhanced mixing and segregation observed in these regions [5–12].

### 2. Variation of tumbler diameter

Another important question is how the length of the flowing layer influences the streamwise and axial velocities of the flowing layer? Figures 4 and 5 [(e)–(h)] indicate that decreasing the flowing layer length by reducing the tumbler diameter causes the axial velocity magnitude to decrease. Figure 11(a) shows the axial velocity profile along the length of the flowing layer at the axial position where the axial velocity magnitude is greatest, $z_{\max}/H$, for 1 mm particles rotated at 2.0 rpm for cylindrical tumblers of different diameters. The velocity profiles appear to collapse reasonably well when scaled with the linear speed of the tumbler ($\omega R$), which, of course, is related to the flowing layer length. This result is not unexpected given that the streamwise velocity also scales with flowing layer length [4,24], as confirmed by the similar streamwise velocities at the axial position $z/H=0$, as shown in Fig. 11(b). The collapse of the velocity profiles is imperfect, particularly near the end wall, but the similarity is clear, especially considering that the tumbler

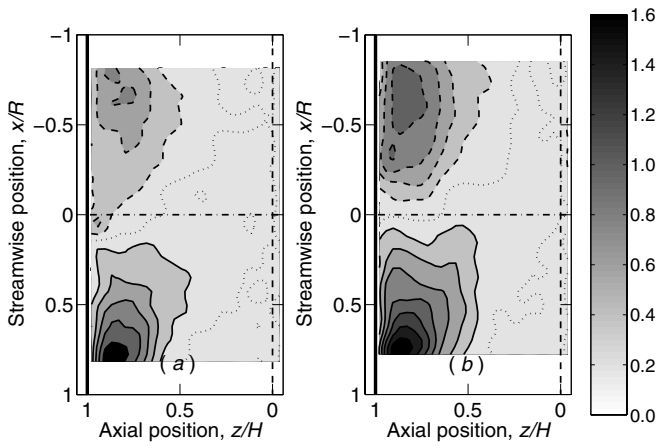


FIG. 12. Spanwise velocity of $L/D=1.03$ cylinder with 1 mm particles rotated at 2.0 rpm for (a) acrylic and (b) sandpaper end walls. Flow is from top to bottom with contours as in Fig. 4.

diameter varies by a factor of 2.4 for the data in Fig. 11(b). Since in all cases the axial length satisfies the $L>D$ condition necessary for localized end-wall effects, the maximum streamwise velocity is located near the end wall and not at the center of the tumbler. The maximum streamwise velocity is faster than the free stream velocity at the center of the tumbler by 16%, 11%, 10%, and 21% for the 7.0-, 10.0-, 14.0-, and 17.0-cm-diam tumblers, respectively, to compensate for the slower streamwise velocity immediately adjacent to the end walls. The axial positions, $z_{\max}/H$, of the axial velocity profile data shown in Fig. 11(a) are indicated by filled data points and show that the axial extent of the boundary flow increases as a function of the flowing layer length.

To confirm that slower velocity adjacent to the end walls is due to frictional interaction between particles and the end-wall surface, the end walls of the $L/D=1.03$ tumbler were covered with 100 grit sandpaper, thus increasing the friction at the end wall. A comparison of frictional influence of the end wall with and without sandpaper on the spanwise velocity contours for 1 mm particles rotated at 2.0 rpm is shown in Fig. 12. The higher axial velocity in Fig. 12(b) indicates that greater friction between the particles and the end wall increases the axial velocity near the end walls. Although the increase in end-wall friction due to sandpaper causes an increase by 30% in the maximum axial velocity near the end walls, it results in only a 6% increase in the maximum streamwise velocity near the end wall from 12.2 to 12.9 cm $s^{-1}$. The rough end walls also result in the streamwise velocity immediately adjacent to the end wall decreasing by an average of 8% along the length of the flowing layer compared to the acrylic end-wall condition. The increase in maximum axial velocity for the 2 mm particles is 26% with only a 1.5% increase in maximum streamwise velocity from 10.9 to 11.1 cm $s^{-1}$. These results indicate that losses are greater due to friction near the end walls, whether it is a result of longer contact with the end-wall surface (increasing tumbler diameter) or a rougher end-wall surface (increasing end-wall friction), causes the particles to move away from the end walls at higher speed, which is related to a higher streamwise velocity in the boundary flow via the

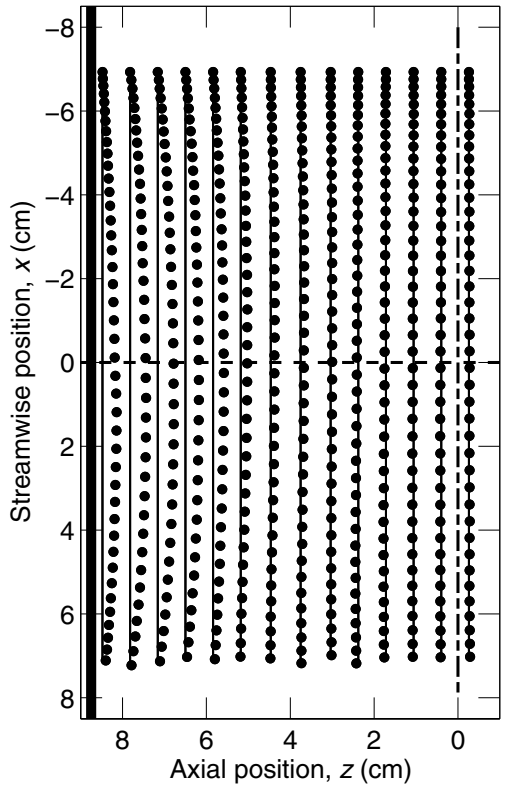


FIG. 13. Tracks of particles started at various axial locations in the $L/D=1.03$ cylinder rotating at 2.0 rpm with 1 mm particles. Flow is from top to bottom. Markers show each 30 ms integration step; the straight lines are along the streamwise direction as a visual guide to show the curvature of the particle tracks.

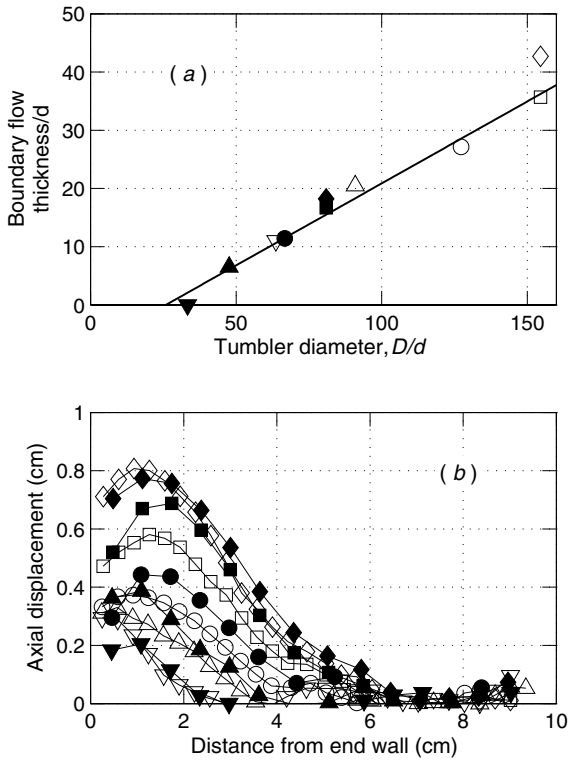


FIG. 14. (a) The relationship between the thickness of the boundary flow based on a displacement of $1.5d$ at the midlength of the flowing layer and the diameter of the tumbler. (b) The axial displacement at the midlength of the flowing layer as a function of the distance from the end wall. Symbols indicate tumbler diameter/end-wall condition for an $L=17.5$ cm tumbler: ▽, 7.0 cm ($L/D=2.5$); △, 10.0 cm ($L/D=1.75$); ○, 14.0 cm ($L/D=1.25$); □, 17.0 cm ($L/D=1.03$); and ◇, 17.0 cm ($L/D=1.03$, sandpaper condition); open symbols for 1 mm particles and filled symbols for 2 mm particles.

conservation of mass. There was, however, no significant change in the streamwise or axial surface velocity at the center of the tumbler for either case indicating that the tumbler is long enough so that the boundary flow region was localized to the end wall despite the increased end-wall friction.

To better understand the motion of particles through the flowing layer, the mean velocity field was used to generate tracks of particle motion at the free surface. Starting with particles positioned at the maximum upstream measurement location, a simple Euler integration scheme was used to track the particles with the streamwise and spanwise velocity components estimated by linear interpolation of the four nearest grid points. The particle tracks for the $L/D=1.03$ cylinder rotated at 2.0 rpm with 1 mm particles are shown in Fig. 13. The particle positions, denoted by markers at each time step of the integration, have larger displacements at the midlength of the flowing layer due to the higher streamwise velocity and shorter displacements at the extremes of the flowing layer due to the slower streamwise velocity. Near the end wall, the particle tracks deviate substantially from pure streamwise motion (the solid line). The paths closer to the center of the tumbler ($z=0$) have negligible axial displacement.

By fitting parabolic profiles to particle paths like those shown in Fig. 13, it is possible to estimate the axial displacement of particles in the flow field as a function of the position in the flowing layer. The "boundary flow thickness" is arbitrarily defined as the maximum distance from the end wall where the axial displacement is at least 1.5 particle diameters at the midlength of the flowing layer (based on the axial distance between the particle path and the vertical lines in Fig. 13). Plotting the thickness of the boundary flow computed in this way, nondimensionalized by the particle diameter, as a function of the tumbler diameter, also nondimensionalized by the particle diameter, collapses the data onto a linear relation, regardless of the particle size, as shown in Fig. 14(a). (The data point for the 7.0-cm-diam cylinder with 2 mm particles is zero, because no particle paths produced an axial displacement of at least $1.5d$.) Clearly, the effect of the end walls can be felt by the flow many particle diameters away from the end walls. The slope of the boundary flow thickness dependence on tumbler diameter in Fig. 14(a) is independent of the arbitrary distance chosen for axial displacement defining the thickness. Changing the value defining the axial displacement for the boundary flow thickness simply shifts the line vertically. The diamond symbols at $D/d=84$ and 159 in Fig. 14(a) are for the 17.0-cm-diam cylinder with sandpaper end walls. The higher friction increases the thickness of the boundary flow. Naturally, the

linear relationship in Fig. 14(a) will reach a limit either when the cylinder diameter is large enough so that the streamwise velocity reaches a terminal velocity or when the axial length is small enough so $L<D$, causing the boundary flows from the two end walls to merge.

While Fig. 14(a) indicates the thickness of the boundary flow region, the axial displacement of particle paths from straight lines at the midlength of the flowing layer depends on the distance from the end walls, as shown in Fig. 14(b). The high axial displacement close to the end wall of the tumbler corresponds to the high axial velocity magnitudes evident in the contour plots of Figs. 4 and 5 [(e)–(h)]. However, particles immediately adjacent to the end walls have smaller axial displacements. Particle collisions with the end wall cause slower streamwise and axial velocities, which corresponds to the decreased axial displacement immediately adjacent to the end wall. Particles in the boundary flow at a given axial distance from the end wall have increased axial displacement as the integrated frictional influence increases via either a longer flowing layer or by a rougher end wall. The dimensional axial displacement is essentially independent of the particle size for the 1 and 2 mm particles that were considered.

#### *3. Variation in tumbler rotation rate*

The data presented in the previous sections were for tumblers rotated at 2.0 rpm. Figure 4(c) also shows the axial velocity contours for the $L/D=0.26$ cylinder for three different rotation rates, $\omega=1.0$, 2.0, and 3.5 rpm. Rotation rates faster than 3.5 rpm were not possible due to the limited time that the opening between edges **A** and **B** was visible in the field of view of the camera. Rotation rates slower than 1.0 rpm resulted in the free surface having intermittent avalanches rather than continuous flow. The variation in rotation rate corresponds to more than an order of magnitude increase in the Froude number from $\mathrm{Fr}=9.5\times10^{-5}$ to $\mathrm{Fr}=1.2\times10^{-3}$. The shape of the axial velocity contours is consistent for the three rotational speeds shown in Fig. 4, but the magnitude increases substantially with increasing rotation rate as indicated by the darker intensity and increased number of contour lines as $\omega$ increases. At $x/R=0.75$, the axial velocity averaged across the axial length of the tumbler doubles when the rotational speed doubles from $\omega=1$ to 2 rpm, and it more than doubles again when $\omega$ increases from 2 to 3.5 rpm. This is consistent with the scaling of the axial velocity with $\omega R$ shown in Fig. 11(a), although the scaling of the axial velocity is not exactly linear with the rotation rate [24].

### C. Nonspherical particles

Experiments were also conducted with nonspherical particles to verify that axial flow is related to the end-wall boundary condition and not the particle shape or size. Black sand that passed through a 0.5 mm mesh was tumbled at 2.0 rpm in the $L/D=0.26$ cylinder. Due to the nonspherical nature of the particles, individual particles could not be identified, making PTV difficult. Therefore, PIV was used to measure the flow field [26–28], albeit with less velocity resolution than with PTV. In addition, it was not possible to accurately measure the velocity in the upstream portion of the flowing layer due to occlusion of edge A after the flow become steady.

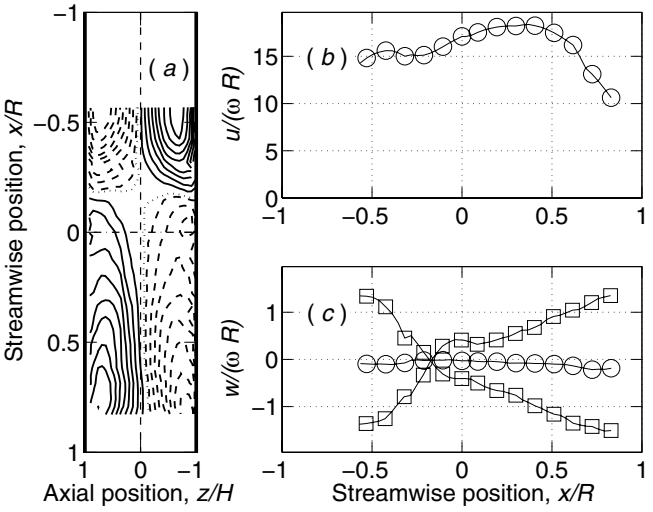


FIG. 15. (a) Axial velocity of the free surface; (b) streamwise velocity profile along the flowing layer at the center of the tumbler; (c) axial velocity profiles along the flowing layer for different axial locations: ○ at the center of the tumbler, □ for $z/H\approx\pm0.75$. Only one-third of the data points are indicated with a marker. Data are for 0.5 mm black sand in the $L/D=0.26$ tumbler rotated at 2.0 rpm. Contours represent steps of 0.3 cm $s^{-1}$. Shading related to axial velocity magnitude is not shown due to the density of contours.

The axial velocity contours and velocity profiles along the flowing layer length are shown in Fig. 15. The contours exhibit the same form as those for the spherical particles. Flow is away from the end wall in the upstream portion of the flowing layer and toward the end wall in the downstream portion, although the axial velocity magnitudes are much higher in this case than for the 1 and 2 mm basalt glass particles in the same tumbler, but consistent with higher velocities for smaller particles. Since $L<D$, the flows at the two end walls interact symmetrically with one another. However, antisymmetry with respect to the midlength of the flowing layer does not occur in this case. The zero axial velocity contour for the sand is offset upstream at $x/R=-0.175$, instead of close to $x/R=0$, as is the case for the spherical particles. This asymmetry is also evident in the streamwise and axial velocity profiles, shown in Figs. 15(b) and 15(c). The streamwise velocity profile does not have the parabolic form that occurs for spherical particles. Instead, the velocity is higher (compared to Fig. 8), and the velocity maximum occurs downstream of the midlength of the flowing layer, at $x/R=0.38$. Additionally, the streamwise velocity is slightly depressed for $-0.32\leqslant x/R\leqslant-0.18$, which may correspond to the zeros in the axial velocity profiles for $z/H=\pm0.75$ in Fig. 15(c).

The different surface velocities likely result from a combination of the effects of particle shape, size, and density. The sand has a slightly higher angle of repose than the glass ($\theta_{\mathrm{sand}}\approx31°$ versus $\theta_{\mathrm{glass}}\approx26°$). Much like an increase in rotation rate causes more energetic particle flow, the higher angle of repose in addition to the small particle size gener-

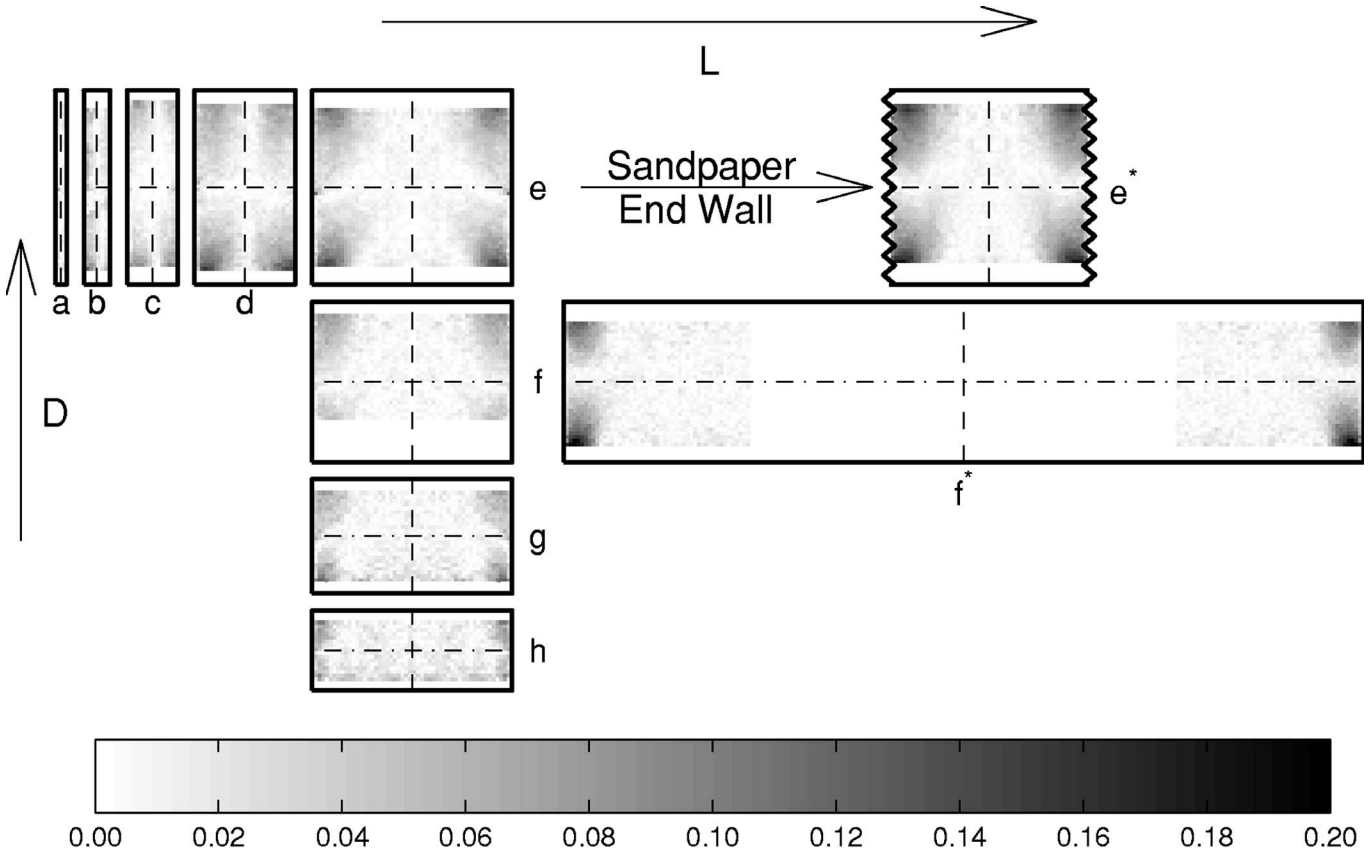


FIG. 16. Ratio of the magnitude of axial flow with respect to the streamwise flow for 1 mm particles in the following tumblers that are drawn to scale: (a) $L/D=0.06$, (b) $L/D=0.14$, (c) $L/D=0.26$, (d) $L/D=0.52$, (e) $L/D=1.03$, (e*) $L/D=1.03$ with sandpaper end-wall conditions, (f) $L/D=1.25$, (g) $L/D=1.75$, (h) $L/D=2.5$, and (f*) $L/D=5.0$. For the longer tumblers, data from the left end wall are reflected about the line of symmetry at the center of the tumbler.

ates greater speed when the particles tumble down the free surface. Furthermore, the sand took a longer time from start-up of the tumbler to reach steady flow compared to the glass particles. The dissimilar flow regimes may contribute to the disparity in the velocity profiles and contours between the glass beads and the sand. The key result, however, is that similar boundary flows occur in a rotating tumbler regardless of significant variations in the granular material.

## IV. CONCLUSIONS

The results presented here have implications on two levels. One aspect is in shedding light on the physics of granular flow. The second concerns practical implications, extending possibly to the design of mixing devices and the like. A key question is, under what conditions can a system be regarded as 2D, and how does this 2D geometry affect the flow compared to a fully 3D condition? A related question is, when is a system large enough that end effects may be regarded as negligible? These questions are important in determining what conditions justify the use of various approximations in modeling studies. The results presented here clarify several aspects of the flow in rotating granular tumblers, but also open many questions. In what follows, we summarize what has been found and identify open questions.

Although the flow of particles at the free surface in rotating tumblers is primarily down the slope of the material and perpendicular to the axis of rotation, there is also a significant axial flow induced near the end walls of the tumbler. The nature of the free surface flowing layer for all tumbler axial lengths and diameters is summarized in Fig. 16, where the intensity of shading represents the magnitude of the ratio of axial velocity to streamwise velocity, $|w/u|$. Dark regions near the end walls show areas where the axial flow is strong and the streamwise velocity is reduced due to frictional interaction. Figure 16 includes data for the tumbler with $L/D=5.0$, although measurements are obtained only within $1.2D$ of the end wall. The darkest intensity is not shown for the shorter tumbler of the same diameter because of the occlusion issue mentioned in the caption of Fig. 4.

It is evident that the size and strength of the boundary flow increases as the flowing layer length (diameter of the tumbler) and the friction at the end walls increase. Clearly, the boundary flow regions are localized near the end walls when the axial length of the tumbler becomes sufficiently large, and they do not interact with each other. The intensity of the boundary flow decreases as the axial length of the tumbler decreases for $L<D$. As the axial length of the tumbler decreases, the two boundary flows merge to produce a faster streamwise velocity in the tumbler than occurs in a long tumbler.

The existence of the boundary flow results in quantitative and qualitative differences between quasi-two-dimensional and three-dimensional tumbler flow. The light regions at the axial center of the tumbler (vertical dashed lines in Fig. 16) have very small axial velocities. While the flow characteristics at the axial center of quasi-2D tumblers and 3D tumblers may appear similar, they are actually a result of very different phenomena. In long axial tumblers (3D), the boundary flows are localized near the end walls, thus there is no driving force for axial velocity at the center of the tumbler. Conversely, in short tumblers (quasi-2D), this zero axial velocity region is due to a symmetric merging of the boundary flow from *both* end walls.

The zero axial velocity regions near the midlength of the flowing layer in Fig. 16 (horizontal dashed lines) are due to the conservation of mass in the flowing layer, regardless of the quasi-two-dimensional or three-dimensional nature of the tumbler. In this case, the axial flow direction is reversing so it is toward the end wall in the downstream region of the flowing layer.

Care is necessary when considering end-wall effects in granular tumblers and in extrapolating quasi-two-dimensional results to three-dimensional cases. There is a remarkable difference in free surface flow between quasi-two-dimensional and three-dimensional tumblers due to the existence of boundary flow from end-wall effects. Figure 17 shows how the maximum streamwise velocity at the axial center of the tumbler decreases as the ratio $L/D$ increases for all tumbler diameters, lengths, rotational speeds, and end-wall conditions. A distinct transition occurs at $L/D \approx 1$. In long tumblers where $L > D$, boundary flow is localized to individual end walls causing a non-negligible axial velocity and a 10–20 % increase in streamwise flow in these regions. However, there is no influence of the end walls on the flow properties elsewhere in the tumbler. The end-wall effects merge when $L < D$. The magnitude of axial velocity is reduced due to merging boundary flows, and the streamwise velocity in the axial center can increase by more than a factor of 2 when the flow is quasi-two-dimensional due to the limited axial space for boundary flow development.

The results presented here are limited to observations of flat, continuous free surface flow of monodisperse particles in rotating tumblers. The axial flow near the end walls may contribute to the formation of axial bands in segregating experiments of bidisperse particles [8–11] and are likely related to the enhanced rate of mixing near the end walls in granular tumblers [12]. Several questions arise. For instance, what is the nature of analogous boundary flows in tumblers that are operating in the avalanching or cataracting flow regimes? Specifically, are the avalanches long enough in duration to interact with the end walls to sustain a measurable axial velocity? Since the axial velocity probably does not increase without bound as the Froude number is increased, is the nature of the boundary flow in the cataracting flow regime similar to that for flat flowing layers? One may also speculate that changes in the fill fraction of the rotating tumbler will alter the axial component in the boundary flow. For tumblers less than half full, particles enter the flowing layer with an initial negative streamwise velocity that may cause the axial velocity or particle paths to exhibit different characteristics from those presented here. Furthermore, the boundary flow in a tumbler suggests that flow may vary along the streamwise direction in chute flow due to side wall effects. Finally, these results indicate that flow in a quasi-two-dimensional system cannot be thought of as simply a slice in a three-dimensional system.

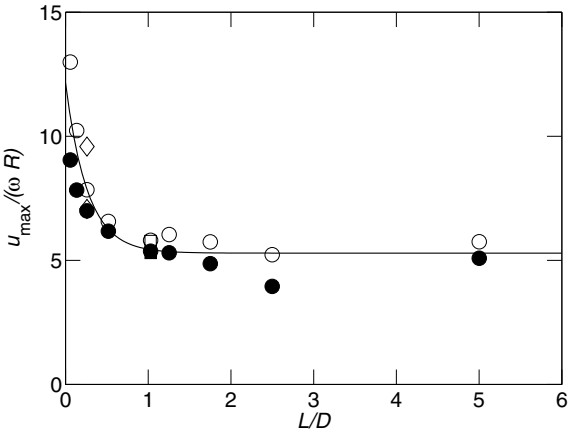


FIG. 17. Maximum streamwise velocity at the axial center of all tumblers tested as a function of $L/D$ for the following operating conditions: ○, varying axial lengths and diameters at 2.0 rpm; □, sandpaper end-wall conditions; ◇, rotation rates of 1.0 and 3.5 rpm; open symbols for 1 mm particles; filled symbols for 2 mm particles. The curve is sketched as a guide to the eye.

## ACKNOWLEDGMENTS

This work was funded in part by the Office of Basic Energy Sciences of the Department of Energy (Contract No. DE-FG02-95ER14534) and by the National Science Foundation IGERT Program "Dynamics of Complex Systems in Science and Engineering" (Grant No. DGE-9987577).

[1] P. Jop, Y. Forterre, and O. Pouliquen, J. Fluid Mech. **541**, 167 (2005).
[2] A. A. Boateng and P. V. Barr, J. Fluid Mech. **330**, 233 (1997).
[3] J. E. Maneval, K. M. Hill, B. E. Smith, A. Caprihan, and E. Fukushima, Granular Matter **7**, 199 (2005).
[4] N. A. Pohlman, S. W. Meier, R. M. Lueptow, and J. M. Ottino, J. Fluid Mech. **560**, 355 (2006).
[5] M. B. Donald and B. Roseman, Int. Chem. Eng. **7**, 749 (1962).
[6] S. Das Gupta, D. V. Khakhar, and S. K. Bhatia, Chem. Eng. Sci. **46**, 1513 (1991).
[7] M. Nakagawa, Chem. Eng. Sci. **49**, 2540 (1994).
[8] K. M. Hill and J. Kakalios, Phys. Rev. E **49**, R3610 (1994).

[9] K. M. Hill and J. Kakalios, Phys. Rev. E **52**, 4393 (1995).
[10] K. M. Hill, A. Caprihan, and J. Kakalios, Phys. Rev. E **56**, 4386 (1997).
[11] S. J. Fiedor and J. M. Ottino, Phys. Rev. Lett. **91**, 244301 (2003).
[12] A. Santomaso, M. Olivi, and P. Canu, Chem. Eng. Sci. **59**, 3269 (2004).
[13] J. Rajchenbach, E. Clement, and J. Duran, in *Powders & Grains 1993*, edited by C. Thornton (A. A. Balkema, Rotterdam, 1993), pp. 333–335.
[14] S. Warr, G. T. H. Jacques, and J. M. Huntley, Powder Technol. **81**, 41 (1994).
[15] V. V. R. Natarajan, M. L. Hunt, and E. D. Taylor, J. Fluid Mech. **304**, 1 (1995).
[16] G. H. Ristow, Europhys. Lett. **34**, 263 (1996).
[17] T. S. Komatsu, S. Inagaki, N. Nakagawa, and S. Nasuno, Phys. Rev. Lett. **86**, 1757 (2001).
[18] N. Jain, J. Ottino, and R. M. Lueptow, Phys. Fluids **14**, 572 (2002).
[19] K. M. Hill, G. Gioia, and V. V. Tota, Phys. Rev. Lett. **91**, 064302 (2003).
[20] A. V. Orpe and D. V. Khakhar, Phys. Rev. Lett. **93**, 068001 (2004).
[21] N. Jain, J. M. Ottino, and R. M. Lueptow, J. Fluid Mech. **508**, 23 (2004).
[22] M. Nakagawa, S. A. Altobelli, A. Caprihan, E. Fukushima, and E.-K. Jeong, Exp. Fluids **16**, 54 (1993).
[23] D. J. Parker, A. E. Dijkstra, T. W. Martin, and J. P. K. Seville, Chem. Eng. Sci. **52**, 2011 (1997).
[24] A. Alexander, T. Shinbrot, and F. J. Muzzio, Powder Technol. **126**, 174 (2002).
[25] E. A. Cowen and S. G. Monismith, Exp. Fluids **22**, 199 (1997).
[26] A. Medina, J. A. Cordova, E. Luna, and C. Trevino, Phys. Lett. A **250**, 111 (1998).
[27] R. M. Lueptow, A. Akonur, and T. Shinbrot, Exp. Fluids **28**, 183 (2000).
[28] A. Medina, J. Andrade, J. A. Cordova, and C. Trevino, Phys. Lett. A **273**, 109 (2000).